Accelerated Joint Image Despeckling Algorithm in the Wavelet and Spatial Domains

Adib Akl *adibakl@usek.edu.lb*
Faculty of Engineering, Department of Telecommunications
Holy Spirit University of Kaslik (USEK)
Jounieh, P.O. Box 446, Lebanon

Charles Yaacoub *charlesyaacoub@usek.edu.lb*
Faculty of Engineering, Department of Telecommunications
Holy Spirit University of Kaslik (USEK)
Jounieh, P.O. Box 446, Lebanon

Abstract

Noise is one of the most widespread problems present in nearly all imaging applications. In spite of the sophistication of the recently proposed methods, most denoising algorithms have not yet attained a desirable level of applicability. This paper proposes a two-stage algorithm for speckle noise reduction jointly in the wavelet and spatial domains. At the first stage, the optimal parameter value of the spatial speckle reduction filter is estimated, based on edge pixel statistics and noise variance. Then the optimized filter is used at the second stage to additionally smooth the approximation image of the wavelet sub-band. A complexity reduction algorithm for wavelet decomposition is also proposed. The obtained results are highly encouraging in terms of image quality which paves the way towards the reinforcement of the proposed algorithm for the performance enhancement of the Block Matching and 3D Filtering algorithm tackling multiplicative speckle noise.

Keywords: Denoising, Spatial Filter, Speckle, Wavelet.

1. INTRODUCTION

Multiplicative in nature, speckle noise is a common problem found in different imaging applications such as ultrasound, sonar and radar imaging [1, 2]. Originating from the superposition of acoustical echoes coming with random phases and amplitudes during acquisition or transmission, it tends to reduce the image resolution and contrast and blur important details [1].

Despeckling can address the multiplicative nature of the noise, or transform the noisy image to the logarithmic domain where multiplicative noise becomes additive, and apply additive noise reduction techniques [2].

In the past decades, several algorithms have been proposed for image denoising. Hybrid order statistics filters for speckle reduction are proposed in [2]. A preprocessing technique is used in order to transform the noise in the logarithmic domain to a Gaussian-like noise, which allows for better filtering results using known denoising techniques [3-5]. Lee [6-8], Kuan [3, 9], and Frost [10] filters are still widely used in many applications. In general, they succeed to reduce speckle in homogenous areas. However, in heterogeneous areas, speckle is retained. Therefore, they are not able to perform a full removal of speckle without blurring any edges because they rely on local statistical data related to the filtered pixel and this data depends on the occurrence of the filter window over an area. Wavelet-based denoising techniques [4, 10, 11, 12] represent the image jointly in the spatial and frequency domains. They rely on the sparse representation of the wavelet sub-bands coefficients in order to be distinctly thresholded. The Block Matching and 3D

Filtering (BM3D) algorithm [13, 14] is a non-local denoising technique in a non-spatial domain. It combines non-local image modeling and the sparse representation of the wavelet domain.

In the following, a two-stage despeckling algorithm is proposed. It consists of jointly denoising the speckled image in the wavelet and spatial domains. At the first stage, the traditional speckle reduction filter of Kuan [3] is adapted to the specificities of the filtered image by estimating its optimal parameter value automatically, based on edge pixels statistics and noise variance. Then the resulting sub-optimal spatial filter is used at the second stage to smooth the approximation sub-band coefficients in the wavelet domain. Since wavelet decomposition is time-consuming when dealing with large sized images, a complexity reduction algorithm is also proposed. Note that the Kuan filter is used as the basis for the spatial filtering due to its versatility. However, other algorithms could be used.

The remainder of this paper is organized as follows. Existing noise reduction methods are reviewed in Section 2. The proposed algorithm is then described in Section 3. In Section 4, results are shown and discussed. Finally, conclusions are drawn and prospects are provided in Section 5.

2. EXISTING NOISE REDUCTION ALGORITHMS

In the past decades, several image denoising algorithms have been proposed. For instance, the spatial means filters (arithmetic mean, geometric mean, harmonic mean and contraharmonic mean filters [15]) smooth the local variations in an image by blurring the noise. The spatial order-statistic filters (median, max, min, midpoint and alpha-trimmed mean filters [15]) are based on ordering (ranking) the values of the pixels contained in the image area encompassed by the filter. The spatial adaptive filters (adaptive local noise reduction and adaptive median filters [15]) change their smoothing behavior based on statistical characteristics of the image inside the filter region. The spatial filters listed above have shown to successfully deal with a large panel of noisy images in situations when only additive noise is present. However, they are not able to reduce speckle noise which is non-additively combined with the underlying image.

Various nonlinear filtering techniques have also been proposed [16]. They seek to reduce the effect of speckle noise while preserving the informative structure of the underlying image. Some of the best known standard speckle noise reduction filters are the methods of Lee [6-8], Gamma [24], Kuan [3, 9] and Frost [24]. These filters use the second-order sample statistics within a minimum mean squared error estimation approach.

2.1 Lee Filter

The locally adaptive Lee multiplicative filter [7, 8] is based on a multiplicative noise image model as follows:

$$g(x,y) = f(x,y) \times n(x,y) \ , \tag{1}$$

where *g* denotes the observed image, *f* the original image and *n* the multiplicative speckle noise [6].

Based on an assumption that the noise is white, with unity mean, and uncorrelated with the image *f*, the multiplicative Lee filter gives the best mean-squared estimate of *f* at each pixel $g(x,y)$ by:

$$z(x,y) = \overline{f} + k_{(x,y)}\left[g(x,y) - \overline{f}\right], \tag{2}$$

where $z(x,y)$ is the filtered pixel, $\overline{f}$ is the mean of the original image pixels under the filtering window (i.e. the local mean) and $k_{(x,y)}$ is the gain factor given by:

$$k_{(x,y)} = \frac{\sigma_f^2}{\overline{f}^2 \sigma_n^2 + \sigma_f^2} \ , \tag{3}$$

where σ_f^2 is the variance of the original image pixels under the filtering window (local variance), and σ_n^2 is the noise variance. The local adaptation of the filter is based on the calculation of the local statistics $\bar{f}$ and σ_f^2 from the data sample estimates $\bar{g}$ and σ_g^2 determined over a local neighborhood window.

This requires the knowledge of the Coefficient of Variation (CoV), which is the ratio of the standard deviation to the mean in homogeneous areas. If the original image is not available, the noise variance can be determined from the number of looks or the Equivalent Number of Looks (ENL). This parameter effectively controls the amount of smoothing applied to the image. The filter size greatly affects the quality of the processed image. If the filter is too small, the noise filtering algorithm is not efficient. If the filter is too large, some details of the image will be lost [17-19].

An improved version of the basic Lee filter also exists; the modified Lee filter which relies on a ratio-based edge detection algorithm used to estimate the edge strength at each pixel in the image [20].

2.2 The Gamma Maximum A Posteriori Filter

The Gamma Maximum A Posteriori (MAP) filter [21] is used primarily to filter speckled radar data while preserving high frequency features. It’s based on a Bayesian analysis of the image statistics. It performs spatial filtering on each individual pixel in an image using the grey level values in a square window surrounding each pixel. The Number of Looks (NLOOK) parameter effectively controls the amount of smoothing applied to the image. It affects the speckle coefficient of variation (C_u) and the upper speckle coefficient of variation $(C_{\max})$. A small NLOOK value leads to more smoothing and a larger NLOOK value preserves more image features.

If $C_i \le C_u$ (C_i is the image variation coefficient), the filtering window is over a homogenous area and smoothing is applied. If $C_i \ge C_{max}$, the filtering window is over an area of high local standard deviation (crossing edge-pixels), and therefore edge-pixel is replicated [24].

If $C_u < C_i < C_{max}$, the filtered pixel value based on the Gamma estimation of the contrast ratios within the appropriate filter window is given by:

$$z(x,y) = \frac{(W - NLOOK - 1)\times \bar{g} + \sqrt{D}}{2\times W}, \quad (4)$$

where:

$W = \frac{1+C_u^2}{C_i^2 - C_u^2}$, $D = \bar{g}^2 \times (W - NLOOK - 1)^2 + 4\times W \times NLOOK \times \bar{g} \times g(x,y)$ and $\bar{g}$ is the mean of the window pixels.

2.3 Kuan Filter

Similarly to the Lee filter, Kuan filter [3, 9, 22] is designed to smooth out speckle noise while retaining shape features in the image by applying the Minimum Mean Square Error (MMSE) criterion and it is applied to the logarithmic transformation of the noisy image. Kuan filter is used primarily to filter speckled radar data. It performs spatial filtering on each individual pixel in an image using the grey level values in a square window surrounding each pixel [24]. The resulting grey-level value for the smoothed pixel is given by:

$$z(x,y) = g(x,y)\times W + \bar{g}\,(1-W)\ , \qquad (5)$$

where *g(x,y)* is the center pixel of the filtering window, $\bar{g}$ is the mean value of intensity within the filtering window, and *W* is a weighting function which depends on the Number of Looks (NLOOK) parameter [23] and given by:

$$W = \frac{1 - C_u^2 / C_i^2}{1 + C_u^2}\ , \qquad (6)$$

where C_u and C_i are the estimated noise variation coefficient and the image variation coefficient, respectively:

$$C_u = \sqrt{\frac{1}{\mathrm{NLOOK}}}, \qquad C_i = \frac{\sigma_g}{\bar{g}}, \qquad (7)$$

where σ_g is the standard deviation of intensity within the filtering window.

Same as the Lee filter case, a small NLOOK value corresponds to a high noise variation and a low *W* and therefore leads to more smoothing, while a larger NLOOK value corresponds to a low noise variation and a high *W* which preserves more image features.

Theoretically, the correct value for NLOOK should be the Equivalent Number of Looks (ENL) of the image. Depending on the application, the user may experimentally adjust the NLOOK value so as to control the effect of the filter [22].

2.4 Frost Filter

Frost method consists in adjusting the filter's parameters according to local area statistics about the target pixel [24]. When uniform regions are filtered, the filter acts as a mean filter and when high contrast regions are filtered, the filter acts as a high-pass filter with rapid decay of elements away from the filter center. Thus, large uniform areas will tend to be smoothed out and speckle removed, while high contrast edges and other objects will retain their values [24]. The frost filter can be considered as an adaptive-weighted-mean filter since it uses an adaptive filtering algorithm, which is an exponential damped convolution kernel that adapts itself to features by computing a set of weighting factors for each pixel within the filtering window as follows:

$$M_n = e^{\left(-\left(DAMP\times\left(\frac{\sigma_g}{\bar{g}}\right)^2\right)\times T\right)}\ , \qquad (8)$$

where *DAMP* is a factor that determines the extent of the exponential damping for the image, σ_g is the standard deviation of the filter window, $\bar{g}$ is the mean value within the window and *T* is the absolute value of the grey level distance between the center pixel and its surrounding pixels in the filter window [24].

The Enhanced Frost filter is an extension to the basic filter that further divides the image into homogeneous, heterogeneous and isolated point target areas [19]. It can significantly improve the ability of speckle mitigation in the vicinity of edges and small features, thus retaining more image details.

2.5 Denoising Using Wavelets

Wavelet transform [25] has been extensively studied in recent years and used for many application domains, mainly in image compression and noise reduction. It consists of a set basis functions used to analyze signals in both spatial and frequency domains simultaneously. The basic functions of the wavelet transform help to isolate signal discontinuities since high pass filtering is used to obtain detail information and low pass filtering is used to retrieve a smoother approximation of the signal, making it possible to analyze the signal at different scales [22].

Multi-resolution processing of the Discrete Wavelet Transform (DWT)

Multi-resolution processing consists in constructing a set of child wavelets from a mother wavelet using scaling and wavelet functions [22]. These two functions form a filter bank consisting of a low pass and high pass filters. The idea of multi-resolution processing through wavelet decomposition is to pass the signal through the filter bank; the signal is decomposed to detail coefficients (output of the high pass filter) and approximation coefficients (output of the low pass filter). Then, the filter outputs are down-sampled by 2 in the purpose of discarding half the samples. The decomposition is repeated to further increase the frequency resolution [25-27].

Application to Image Denoising

Considering an image corrupted by an additive noise and modeled as $g = f + n$, where f denotes the unknown, noise-free image and n the noise [28, 29], wavelet-based denoising (*Figure 1*) consists in:

1) Applying the DWT to g.
2) Thresholding the detail coefficients (Wavelet shrinkage).
3) Inverse transforming (IDWT) the result to obtain an estimation z of the original image f.

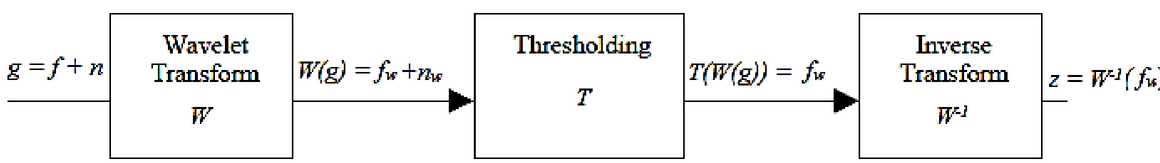

FIGURE 1: DWT Denoising Block Diagram.

When dealing with speckled images, a logarithmic transformation is applied to the noisy image before wavelet decomposition, to transform the multiplicative noise, into additive noise and after wavelet reconstruction, an exponential transformation is applied to reverse the logarithmic operation.

In wavelet domain, the output of the low pass filter consists of the high magnitude and low frequency components (approximation coefficients) and the output of the high pass filter consists of the low magnitude and high frequency components (detail coefficients). *Figure 2* shows a one level, 2D wavelet decomposition scheme [30] where L(.) represents the low pass filtering operator, and the subscript ($_L$) represents a low pass filtered output. Similarly, H(.) and the subscript ($_H$) represent high pass filtering and a high-pass filtered output, respectively. The symbol (↓2) represents a down-sampling operator by a factor of 2.

As a result of filtering and down sampling (*Figure 2*), four sub-bands are obtained: scaling (approximation) coefficients (g_{LL}), horizontal detail coefficients (g_{HL}), vertical detail coefficients (g_{LH}) and diagonal detail coefficients (g_{HH}). The (HL), (LH) and (HH) sub-bands, represent the high frequency (and low magnitude) components and the (LL) sub-band represents the low frequency (and high magnitude) components. At the next level of decomposition, only the (LL) component is passed to the decomposition process.

The reconstruction process or the Inverse Discrete Wavelet Transform (IDWT) consists of assembling back the wavelet coefficients to the original image. After each inverse low and high pass filtering, an up-sampling process (zeros insertion) is required to reverse the decomposition process.

The main idea of wavelet denoising is to threshold only the high frequency components while preserving most of the features in the image by retaining the approximation sub-band.

There are two thresholding methods frequently used; hard [26, 31] and soft [32] thresholding. In hard thresholding, the input is kept if its amplitude is greater than a threshold *T*, otherwise it is forced to zero. In soft thresholding, if the absolute value of the input is less than or equal to a threshold *T*, then the output is forced to zero, otherwise, the output is a scaled version of the input.

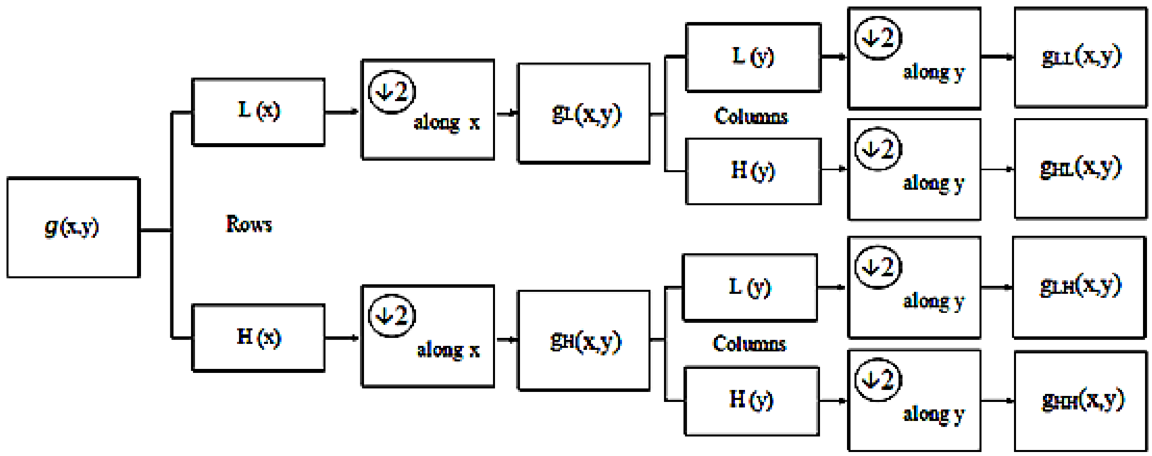

FIGURE 2: One level, 2D Wavelet Decomposition Block Diagram.

Finding a suitable threshold is an important task in wavelet shrinkage. In fact, choosing a very large threshold will shrink to zero almost all coefficients, which results in over smoothing the image, while choosing a very small threshold will yield a noisy result which is close to the input [29]. VisuShrink [25] is an approach that uses a Universal (global) threshold applied to all sub-bands and scales after decomposition [33]. However, this threshold can be unwarrantedly large because it depends on the number of pixels yielding overly smoothed images. In addition, it ignores the difference between sub-bands at different scales [34]. BayesShrink [25, 31] is a sub-band adaptive threshold selection technique that determines a specific threshold for each sub-band assuming a Generalized Gaussian Distribution (GGD) [35]. This method depends on the standard deviation of the noise-free image, and the GGD shape parameter [34]. The method consists of finding, for each sub-band, a threshold that minimizes the expected value of the mean square error (Bayesian Risk) [32, 36].

2.6 The Block Matching and 3D Filtering (BM3D) Algorithm

The BM3D algorithm is a non-local denoising technique [13, 14] in a non-spatial domain. It combines non-local modeling and the sparse representation of the wavelet domain. The algorithm is divided into three processing stages: Block matching, 3D filtering, and aggregation.

In the block matching stage, the noisy image *g* is divided into blocks $G_{x\in X}$ where *x* represents the position of each block in the whole image *X*. For each block, the patches with most resemblance are grouped in a 3D array. Therefore, groups whose elements have a high degree of similarity are constructed separately. Two patches are similar if the Euclidean distance between them is less than a given threshold [14, 37]. The block matching advantages are the induction of a high correlation in the third dimension of the 3D array and the improvement of the dispersion of all possible configurations of details present in the image [13].

3D filtering is a procedure that jointly filters a group of similar blocks by exploiting the similarities between the grouped images and inside each image in the group. It consists of three different sections: 3D transform, shrinkage and inverse 3D transform. Those three procedures are jointly applied [13] on the block. The 3D transform consists of applying a 2D wavelet transform on each patch of the block then a 1D wavelet or Discrete Cosine Transform (DCT) on the resulting patches. As a result of the sparse representation given by the 3D transform, the shrinkage process can effectively attenuate the noise by eliminating the coefficients relying under a certain chosen threshold. The inverse 3D transform consists of assembling back the thresholded coefficients to reconstruct the 3D block.

Finally, the aggregation stage consists of combining the patches in the 3D filtered groups including the reference patch. A trivial solution is to compute the weighted mean of all the estimated patches overlapping at a pixel position [13].

3. THE PROPOSED WAVELET/SPATIAL DESPECKLING ALGORITHM

In this section, a two-stage despeckling algorithm which consists in jointly denoising the corrupted image in the wavelet and spatial domains is proposed. At the first stage, an automatic estimation of the optimal Kuan filter parameter value based on edge pixels statistics and noise variance is developed. Then the resulting adaptive filter is used at the second stage to spatially smooth the approximation sub-band coefficients in the wavelet domain. Since a large number of wavelet levels makes the despeckling algorithm computationally expensive, a complexity reduction algorithm for wavelet decomposition is also proposed. Note that the proposed enhancement targets the Kuan filter due to its versatility and adaptability to speckle noise strength, while a similar study could have been performed with another spatial despeckling method to be used in the hybrid filter that will be discussed in Section 3.2; we therefore focus on the Kuan filter without loss of generality.

3.1 The Adaptive Spatial Filter

As explained earlier, Kuan filtering relies on the Number of Looks (NLOOK) parameter which significantly affects the filtering performance and is usually taken equal to the Equivalent Number of Looks (ENL) of the image. This parameter is manually adjusted, in order to control the strength of the smoothing applied to the image.

We start by implementing the additive model of the Kuan filter using a set of test images (e.g. Lena, Mandrill, LivingRoom, … [38]) corrupted by speckle noise with different distributions. By setting NLOOK = ENL, we notice that filtered images are over-blurred, that's why came our idea of analyzing the Kuan filter performance with respect to the NLOOK parameter and proposing a novel technique for selecting a suitable NLOOK value that yields near-optimal performance compared to manual parameter selection, therefore eliminating the need for several runs of the filter to reach the optimal performance. In this purpose, we define the adjusted NLOOK value as:

$$NLK\_AD = (1 + A)ENL \ , \quad (9)$$

where *A* is the adjustment coefficient.

Figure 3 shows an example of the Lena image filtered with NLOOK=ENL (middle) and NLK_AD as defined in (9), for *A* = 0.65 (right). It can be clearly seen that the image with the adjusted NLOOK parameter (NLK_AD) is much sharper and its details are better preserved.

In the first part of this study, we aim at finding a closed form expression for the adjustment coefficient that yields near optimal performance, without the need for several runs of the filter with different NLOOK values. Therefore, we consider the effect of the filter window size, the image detail, the noise distribution and the noise variance on the optimal adjustment coefficient *A* and consequently, the NLK_AD parameter. Thus, all the listed parameters are fixed and the effect of varying each one of them is studied.

FIGURE 3: Kuan filter results with different NLOOK values. Gaussian and Uniform noise distributions are used in the top and bottom rows respectively. Each row shows (from left to right): the noisy image, the Kuan filtered image using NLOOK=ENL and the corresponding Kuan filtered image using NLK_AD with A=0.65. An 11×11 window with images of size 256×256 are used.

Effect of the Algorithm Parameters on the Optimal Adjustment Coefficient

A Gaussian speckle noise having a variance of 2600 is added to the Cameraman image [38] in order to find the adjustment coefficient A that yields the best result using different window size. The Peak Signal-to-Noise Ratio (PSNR) and the Signal to Mean Squared Error (S/MSE) variations with respect to the NLK_AD parameter are plot and ensure that, for different odd-sized filter windows, the optimal values of A are nearly constant.

On the other hand, test images are distorted with multiplicative speckle noise using the Uniform, Gaussian, Rayleigh, and Erlang distributions while fixing all the other parameters and the optimal value of A remains the same regardless of the noise distribution, for each test image.

In the purpose of studying the influence of the image itself on the filtering process, the filter is applied on different images, having different features, from [38] and [39] with all the other parameters being fixed. It can be noticed that the optimal adjustment coefficient varies with image details. For example, the Pirate image [38] has a high percentage of edges, therefore, the obtained optimal adjustment coefficient is greater than with the Lena image, which is expected since more image features have to be preserved.

To find the relationship between the optimal adjustment coefficient A and the amount of image detail, edge detection is performed on the set of images and the curves presenting the optimal A with respect to the noise variance and the number of edge pixels in each image are drawn.

The Logarithmic and Polynomial Approximations

Since the noise variance affects the filtering process, the variation of A with the noise variance and image detail is modeled as:

$$A = A_d + A_v \text{ ,} \tag{10}$$

where A_d and A_v are the detail and the noise variance components in A, respectively.

We observe that a higher noise variance corresponds to a lower value of A, which is expected since a lower A value leads to more smoothing. Additionally, a higher noise variance corresponds to higher edge percentage (P_e) values because the edge detection algorithm cannot completely differentiate between noise and small edges. Curves for different noise variances have similar behavior with respect to the percentage of edges in the image, therefore, we take as reference one of the curves (for a given variance).

The curve with the solid dark line in *Figure 4* shows the measured A_d with respect to Pe. It can be seen that, for Pe exceeding 2%, A_d varies in a logarithmic or second order polynomial fashion. The former can be expressed as:

$$A_d = \alpha \ln(P_e) + \beta \ , \tag{11}$$

and the latter as:

$$A_d = \lambda P_e^{\,2} + \delta P_e + \mu \ , \tag{12}$$

where α = 0.4015, β = 0.054, λ = –0.01215, δ = 0.20512 and μ= –0.01394 determined by fitting the measured results with (11) and (12) using the Least Squares method.

It can be observed in *Figure 4* that, as the image detail (Pe) increases, A_d increases and consequently, NLK_AD increases. Therefore, less smoothing is performed, as expected. The logarithmic and polynomial approximations mainly overlap with measured data, except for Pe < 2%, which proves high accuracy of the models in (11) and (12).

A similar study with respect to the noise variance shows that A_v (*Figure 5*) can be accurately modeled by a second order polynomial as:

$$A_v = a(v - 2100)^2 + b(v - 2100) \ , \tag{13}$$

where $a = -2\text{x}10^{-8}$ and $b = -42\text{x}10^{-6}$ determined by curve fitting.

Note that for v = 2100, A_v = 0. In fact, A_v reflects the variation of the adjustment coefficient with respect to the noise variance compared to the reference v = 2100 which has been used to derive A_d in (11) and (12). On the other hand, A_v decreases as v increases, which is also expected since more smoothing is required (lower value of NLK_AD) when the noise increases.

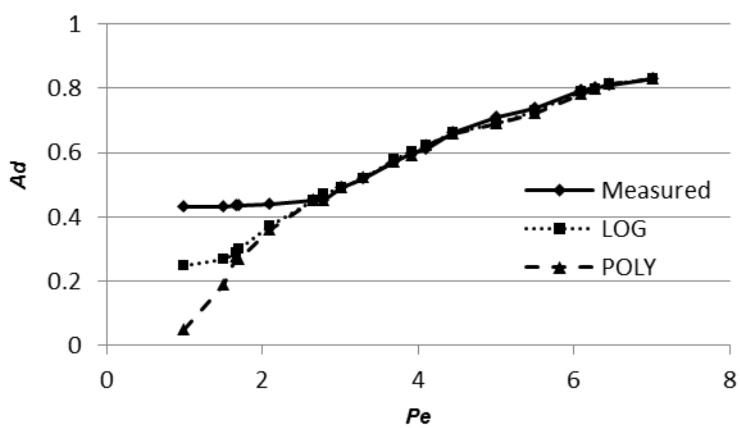

FIGURE 4: Measured and approximated values for A_d for a noise variance of 2100.

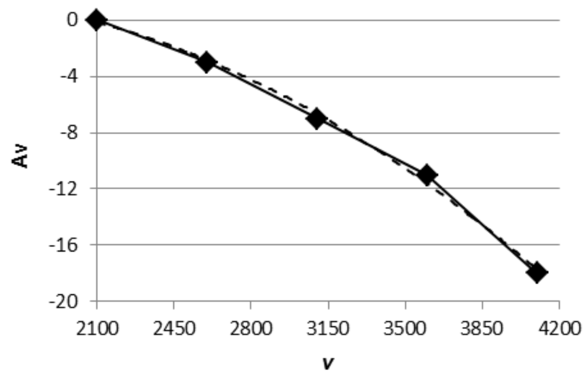

FIGURE 5: Measured (solid line) and approximated (dashed line) values for A_v.

3.2 The Hybrid Wavelet-Spatial Filter

In wavelet denoising, only detail coefficients are thresholded and approximation coefficients remain stagnant, as explained earlier. This is intuitive since the approximation component is a low-frequency image, usually assumed to be noise-free. In fact, this is only a theorectical aspect since practically, approximation coefficients also contain speckle noise as it can be clearly observed in the example shown in *Figure 6*. Wherefore, the proposed algorithm consists of smoothing the approximation coefficients in addition to detail coefficients thresholding as follows:

1) Applying the Discrete Wavelet Transform to the speckled image.
2) Thresholding the detail coefficients (Wavelet shrinkage).
3) Spatial Smoothing of the approximation sub-band coefficients.
4) Applying the Inverse Discrete Wavelet Transform to the result.

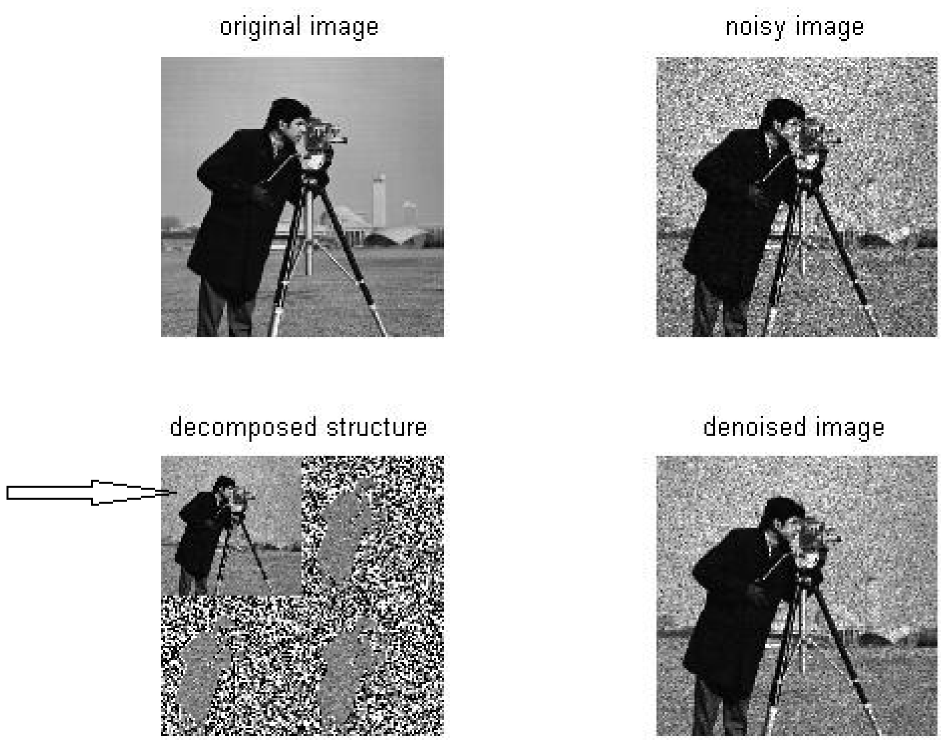

FIGURE 6: Cameraman image of size 512×512 (up-left) [38], corrupted by speckle noise of unit mean and a variance of 2400 (up-right), decomposed structure (down left) and the denoised image (down right). Note the existence of noise in the approximation image of the decomposed structure and the remaining noise in the denoised image (using sym1 wavelets with BayesShrink threshold selection).

An important issue in the approximation image spatial smoothing would be the preservation of the image characteristics. In other words, the algorithm must efficiently smooth out the noise in the approximation image without blurring its details or reducing the contrast and quality. Otherwise, the image structure and dynamics would be lost. Therefore, the approximation sub-band coefficients in the wavelet domain are smoothed using the previously developed adaptive Kuan filter which leads to a better speckle removal without image distortion, as will be seen in Section 4.

3.3 The Proposed Wavelet Acceleration Algorithm

This section deals with accelerating the wavelet filtering process used in the proposed method. The acceleration algorithm consists in finding the number of decomposition levels that yields near optimal performance, without the need for several runs of the wavelet filter with different number of decomposition levels, regardless of the image size, its edge percentage, the noise variance, the wavelet type and base, the wavelet threshold selection technique and the wavelet thresholding technique.

Relative Difference Threshold Selection

We start by applying 100 times, wavelet denoising on an image corrupted by Gaussian speckle noise using different number of decomposition levels (from 1 level to the maximum number of decomposition levels calculated as in [40]). For every run, the simulated speckle noise is regenerated and the PSNR, the Coefficient of Correlation (CoC) and the ENL metrics of the denoised image are calculated and saved.

The second step is the calculation of the relative difference between the ENL of each two consecutive decomposition levels, for the purpose of finding a reasonable relative difference threshold that allows the algorithm to stop before reaching the maximum number of decomposition levels, without loss in performance. The same is performed for different images from [38] and [39], different noise variances (2500, 2600, 3000, 3100, 3500, 4100, 4600 and 6000), different image sizes (128×128, 256×256, 512×512 and 1024×1024), different wavelet types and bases (db2, db4, db7, sym1, sym2 and sym6) and using bayesShrink threshold selection.

After analyzing the results, we noticed that a relative difference smaller than 0.2 leads to an approximately steady PSNR value. As a result, 0.2 is taken as a threshold. Therefore, our proposed algorithm consists of applying a level of wavelet decomposition and denoising, computing the relative difference between the corresponding ENL and the ENL of the previous decomposition level, and stop when the relative difference becomes less than 0.2 as shown in *Figure 7*.

By limiting the number of decomposition levels, a computational gain is expected at the expense of some loss in image quality, as will be shown in Section 4.

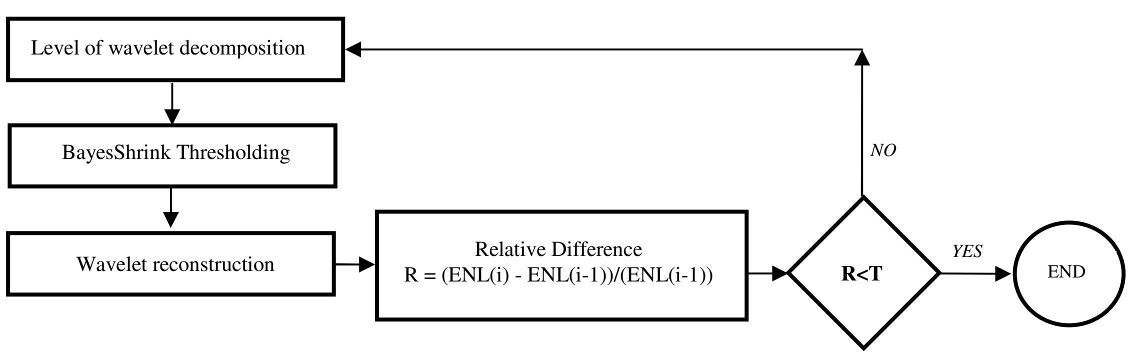

FIGURE 7: Flowchart of the Proposed Acceleration Algorithm.

4. PRACTICAL RESULTS

In this section, the proposed algorithms are put in practice. Besides the subjective qualitative evaluation based on human perception, a quantitative analysis is essential. Thus, an objective benchmark is used to study the quality-related outcomes of the filtering process. Namely, the Peak Signal-to-Noise Ratio (PSNR), the Signal-to-Mean-Squared-Error (S/MSE), the Coefficient of Correlation (CoC) and the Equivalent Number of Looks (ENL).

Peak Signal-to-Noise Ratio (PSNR)

PSNR is considered to be the least complex metric, as it defines the image quality degradation as a plain pixel by pixel error power estimate. PSNR is an engineering term for the ratio between the maximum possible power of a signal and the power of corrupting noise that affects the fidelity of its representation [17]. In image processing, the signal is the original image, and the noise is the error (blur) introduced by the denoising procedure.

Signal-to-Mean Squared Error (S/MSE)

In order to quantify the achieved performance improvement, the Signal-to-Mean Squared Error can also be computed, based on the original and the noisy/denoised images as follows:

$$S/MSE = 10\log_{10}\left(\frac{\sum_{i=0}^{m-1}\sum_{j=0}^{n-1}\left[I(i,j)\right]^2}{\sum_{i=0}^{m-1}\sum_{j=0}^{n-1}\left[K(i,j)-I(i,j)\right]^2}\right), \tag{14}$$

where I is the original image and K the noisy or denoised image. This measure corresponds to the classical SNR in the case of additive noise [41].

Coefficient of Correlation (CoC)

In ultrasound imaging, it is important to suppress speckle noise while at the same time preserving the edges of the original image that often constitute features of interest for diagnosis. For this reason, we also considered a qualitative measure for edge preservation, the Coefficient of Correlation (CoC) metric:

$$CoC = \frac{\Gamma\left(\Delta_I - \overline{\Delta_I}, \Delta_K - \overline{\Delta_K}\right)}{\sqrt{\Gamma\left(\Delta_I - \overline{\Delta_I}, \Delta_I - \overline{\Delta_I}\right).\Gamma\left(\Delta_K - \overline{\Delta_K}, \Delta_K - \overline{\Delta_K}\right)}}, \tag{15}$$

where Δ_I and Δ_K are the high-pass filtered versions of I and K respectively, obtained with a 3×3 pixel standard approximation of the Laplacian operator [25], $\overline{\Delta_I}$ is the mean value of Δ_I and $\overline{\Delta_K}$ is the mean value of Δ_K and the operator Γ is given by:

$$\Gamma(I,K) = \sum_{i=0}^{m-1}\sum_{j=0}^{n-1} I(i,j).K(i.j), \tag{16}$$

where $m\times n$ is the size of the corresponding images I and K.

The CoC cannot exceed 1 in absolute value. It is 1 in the case of an increasing linear relationship and - 1 in the case of a decreasing linear relationship. Its value lies in between in all other cases, indicating the degree of linear dependence between the images. The absolute value of the correlation measure should be close to unity to an optimal effect of edge preservation [41].

Equivalent Numbers of Looks (ENL)

The Equivalent Number of Looks is also a good approach for either estimating the speckle noise variance in a noisy image (in general a SAR image), or evaluating the performance obtained after filtering. ENL is often calculated over a uniform region, but due to difficulties in identifying uniform areas, the image is divided into small areas of 25 x 25 pixels, the ENL is computed for each area

(17), then the average of these ENL values is taken as explained in [12]. Note that this latter method is used throughout this paper. A large ENL value usually corresponds to a better performance. The formula for the ENL calculation is given by:

$$ENL = \left(\frac{\text{mean}}{\text{standard deviation}} \right)^2 . \tag{17}$$

Note that PSNR, S/MSE, and CoC are quantitative metrics, they are based on a pixel by pixel calculation and the original image is needed for computation, whereas ENL is based on the mean and standard deviation, and it can be computed without the need of the original image [22].

4.1 The Performance of the Proposed Adaptive Spatial Filter

It is trivial that a good performing spatial filtering is necessary to get a denoised image of good quality using the proposed approach. Otherwise, the image characteristics will be lost. In this section, the NLOOK parameter estimation previously developed is exploited and compared to the results obtained with the optimal NLOOK value determined manually. Simulations were performed using different standard images from [38] and [39], corrupted by speckle noise of variance ranging from 2100 to 4100. Since many of the samples lead to an approximately same percentage (*Pe*) of edge pixels, and therefore to a similar algorithm behavior, table 1 summarizes sample results obtained for 8 different images having different *Pe* values.

It can be observed that, except for *Pe* < 2 (e.g. Lady image), both the logarithmic and polynomial estimations result in near optimal values for the adjustment parameter, and the PSNR loss does not exceed 0.33 dB and 0.16 dB with logarithmic and polynomial estimations, respectively. In fact, the behavior of the filter when dealing with few-detailed images (Lady image in table 1) is expected, since both proposed approximations fail to be accurate in cases of very low *Pe* values as shown in *Figure 4*. However, images with a percentage of edge pixels less than 2 rarely exist (in our test datasets from [38] and [39], only 11% of the images had *Pe* < 2). Furthermore, the approximation error can be largely reduced by setting A_d to a constant value (approximately 0.43) for such low values of *Pe* as implies *Figure 4*.

It is important to mention that experimental results with such high noise variances are shown to highlight the decent behavior of the proposed method in critical conditions. Moreover, when dealing with slightly speckled images, no filtering is performed (W ≈ 1 in (5)), as will be verified in section 4.2.

Figure 8-a shows the Cumulative Density Function (CDF) of the PSNR loss obtained with both estimations, using the whole set of test images. It can be noticed that in both methods, 50% of the filtered images undergo a loss in PSNR not exceeding 0.05 dB, whereas 85% and 89% undergo a PSNR loss that does not exceed 0.11 dB in logarithmic and polynomial approximations, respectively.

Even though values of *Pe* are more likely to occur between 2% and 8%, let us analyze the proposed models' behavior for values of *Pe* outside this interval. It can be deduced from *Figure 4* that for low values of *Pe*, the measured A_d seems to saturate at a value close to 0.43, while the logarithmic approximation reaches 0 for values of *Pe* close to 0.9% as shown in *Figure 8-b*, and becomes negative for lower values.

Similarly, the polynomial approximation also fails to model A_d at low values of *Pe*, but results in slightly better performance compared to the logarithmic model. This problem can be solved by using any of the two models only when *Pe* exceeds a fixed threshold (e.g. for *Pe* ≥ 2%), or by setting A_d to a constant value (e.g. A_d = 0.43) when *Pe* is below that threshold. On the other hand, the polynomial approximation reaches a peak for *Pe* ≈ 8.5%, and then decreases as *Pe* increases. Therefore, the polynomial model becomes inaccurate in this case. The same does not occur with the logarithmic approximation since it keeps increasing as *Pe* increases.

Noise variance	Image	Pe (%)	Speckled Image PSNR	Log approximation			Polynomial approximation			Optimal values		
				100xA	NLK_AD	PSNR	100xA	NLK_AD	PSNR	100xA	NLOOK	PSNR
2100	Lady	0.9719	26.1012	4.2606	12.1041	24.276	17.393	13.6457	25.695	42	16.5228	28.246
	WomanDarkHair	2.6634	20.6058	44.7361	30.1964	29.115	44.617	30.1987	29.152	44.617	30.1987	29.152
	I06	3.1488	20.5841	51.2811	28.3623	27.569	52.98	28.2943	27.963	53.321	28.5143	27.988
	Lena	4.4518	20.7322	65.3613	28.6966	27.766	65.837	28.8355	27.765	65.3613	28.6966	27.766
	Board	6.0764	19.6519	77.8522	26.12	24.224	78.376	26.349	24.237	78.376	26.349	24.237
	I13	6.2301	21.5436	79.2398	24.9994	26.599	73.987	24.9655	26.541	78.595	24.4561	26.632
	LivingRoom	7.0168	20.9285	83	28.1954	25.992	82.703	28.0957	26.012	83.63	28.4462	26.028
	Mandrill	11.597	20.5485	103.801	30.417	24.865	73.053	25.8463	24.713	103.801	30.417	24.865
2600	Lady	0.9887	25.2349	2.3487	10.611	24.451	15.098	11.9622	25.912	43	14.8931	28.838
	WomanDarkHair	3.0743	20.8759	47.8966	26.4071	28.423	47.58	26.3707	28.435	44	25.7209	28.493
	I06	3.3248	19.6843	52.0432	23.9424	27.107	50.524	23.5761	27.132	50.819	23.5999	27.281
	Lena	4.5025	19.855	63.216	24.2587	27.195	65	24.5917	27.199	63.726	24.4509	27.2
	Board	6.0455	18.7322	73	22.0966	23.658	75.598	22.5739	23.668	75.048	22.4301	23.698
	I13	6.2467	20.5233	74.9848	22.1354	26.260	75.935	22.2013	26.191	75.213	22.5847	26.261
	LivingRoom	6.5968	20.041	78.5514	23.8295	25.51	82	24.4238	25.512	78.436	23.787	25.57
	Mandrill	11.382	19.6209	100.451	26.1791	24.308	72.045	22.5894	24.322	83	23.8904	24.365
3100	Lady	0.9901	24.5231	-1.1945	9.3747	24.321	11.523	10.5359	25.819	40	13.2466	29.024
	WomanDarkHair	3.027	20.177	43.674	22.3196	27.926	43.361	22.2835	27.985	41	21.8922	28.119
	I06	3.5269	18.9928	45.997	19.767	26.501	45.624	19.5671	26.663	51.407	20.223	26.614
	Lena	4.4182	19.1324	58.8572	20.8946	26.767	62	21.2741	26.724	59.31	20.8339	26.785
	Board	6.339	18.0201	73.3508	19.8109	23.235	69	19.2277	23.228	73.601	19.7984	23.266
	I13	6.356	19.8108	75.473	19.4415	25.622	74.423	19.4445	25.992	74.337	19.5426	25.874
	LivingRoom	7.2327	19.2983	78.6463	21.3184	25.078	77.193	21.1876	25.087	76	20.8615	25.121
	Mandrill	12.095	18.9053	99.2916	23.3454	23.803	62.725	19.2675	23.891	79	21.0759	23.956
3600	Lady	0.9953	23.9122	-5.5841	8.2428	24.029	7.0173	9.2931	25.582	36	11.8257	28.94
	WomanDarkHair	3.1719	19.5572	40.9514	19.5081	27.608	40.641	19.6611	27.589	37	18.9953	27.672
	I06	3.6442	18.3526	43.3436	17.2142	26.201	43.221	16.8099	26.204	49.012	17.5012	26.254
	Lena	4.5715	18.5216	55.6266	18.2715	26.398	56.18	18.363	26.464	56.18	18.363	26.464
	Board	6.3707	17.4144	68.9511	17.4682	22.829	69.161	17.6717	22.837	65	17.0354	22.845
	I13	6.4014	19.0212	70.3316	17.9968	25.596	70.44	17.2634	25.526	72.256	17.1994	25.598
	LivingRoom	7.1453	18.7005	73.5582	18.6148	24.753	72.328	18.5073	24.736	72	18.5868	24.797
	Mandrill	11.821	18.2575	93.7692	20.7329	23.4	60.474	17.1004	23.621	73.55	18.5456	23.6257
4100	Lady	0.9971	23.4004	11.1116	7.1373	23.456	1.4499	8.1364	25.193	35	10.8747	29.183
	WomanDarkHair	3.2227	19.0674	35.9893	16.9639	27.374	35.689	16.9408	27.299	35.9893	16.9639	27.374
	I06	3.618	17.7216	38.2526	14.7722	25.921	38.221	14.7677	24.999	44.098	15.2344	25.923
	Lena	4.7283	17.9916	51.3807	16.1424	26.11	52.024	16.1452	26.118	52.024	16.1452	26.118
	Board	6.3188	16.8767	63.0227	15.4386	22.472	63.297	15.4994	22.455	57	14.8499	22.531
	I13	6.3904	18.7049	64.2214	15.9697	25.455	64.031	15.0996	25.402	60.215	15.0027	25.491
	LivingRoom	7.9094	18.1322	72.0373	16.8162	24.427	68.422	16.5037	24.457	66	16.2858	24.465
	Mandrill	12.867	17.733	91.5761	18.8708	23.045	44.941	14.2858	23.313	67	16.3813	23.372

TABLE 1: Summary of results obtained with different 512×512 speckled images using the proposed adaptive spatial filter.

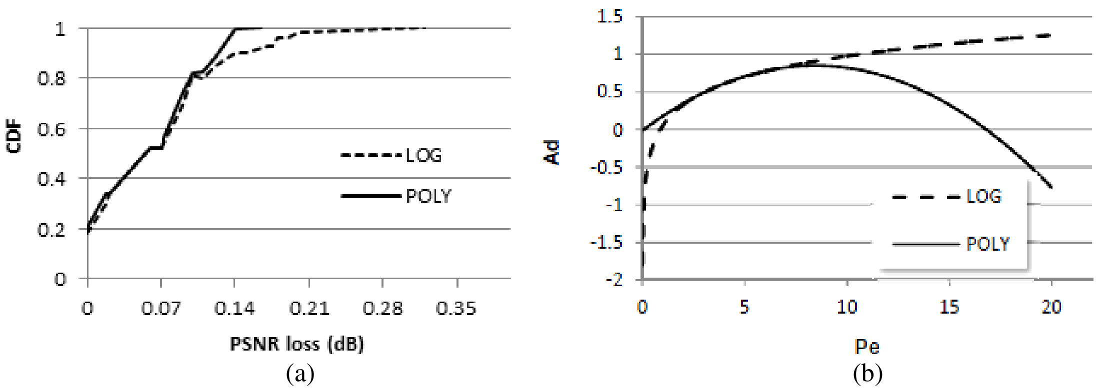

FIGURE 8: (a) CDF of the loss in PSNR due to logarithmic (dotted line) and polynomial (solid line) approximations. (b) Logarithmic (dashed line) and polynomial (solid line) approximations as defined in (11) and (12).

Table 2, 3, 4 and 5 show a comparison of the Lee filter, standard (NLOOK=ENL) Kuan filter, Gamma filter, Frost filter, Enhanced Frost filter, and the proposed enhanced Kuan filter using both the logarithmic and polynomial approximations with a speckle noise of Gaussian, Uniform, Rayleigh and Exponential distributions respectively.

The same is performed for different images of different edge percentage and the results were approximately similar. It can be clearly seen that the performance of the filters is affected by the noise distribution. For the examples shown in Tables 2-5, the Lee multiplicative filter performs better than the Enhanced Frost filter with Uniformly distributed noise, and worse with Gaussian noise, the Kuan filter gives better results than the Lee multiplicative filter except for the case with NLOOK=ENL (where this latter parameter is not adjusted). Depending on the noise distribution, either of the approximations (logarithmic or polynomial) can outperform the other in Kuan filtering with adjusted NLOOK parameter.

In tables 2-5, it can also be observed that the best PSNR is obtained with either the Gamma MAP filter or the proposed (modified) Kuan filter, whereas the Frost and enhanced Frost filters preserve image features more than other filters as it can be noticed from CoC values.

	PSNR	**S/MSE**	**CoC**	**ENL**
Gaussian noise				
Noisy image	19.2482	13.5918	0.1781	13.3615
Lee multiplicative filtered image	26.9749	21.3185	0.3028	98.0283
Kuan filtered image(NLOOK=ENL)	22.8675	17.2111	0.1155	31.6124
K.filtered image (Log. approximation)	27.2248	21.5685	0.3106	106.6198
K.filtered image (Poly. approximation)	27.2389	21.5826	0.3154	110.6581
Gamma filtered image	28.1836	22.5272	0.3892	233.4135
Frost filtered image	26.3968	20.7404	0.4225	233.3297
Enhanced Frost filtered image	27.0823	21.4259	0.4394	240.8940

TABLE 2: Comparison of speckle noise filtering techniques on a 512×512 Lena image corrupted by a Gaussian speckle noise using an 11×11 window size.

	PSNR	S/MSE	CoC	ENL
Uniform noise				
Noisy image	19.1606	13.5042	0.1760	13.1826
Lee multiplicative filtered image	27.5563	21.9000	0.3348	131.8801
Kuan filtered image(NLOOK=ENL)	23.0604	17.4040	0.1210	33.0601
K.filtered image (Log. approximation)	27.7578	22.1015	0.3420	144.8634
K.filtered image (Poly. approximation)	27.7968	22.1405	0.3403	145.0305
Gamma filtered image	27.3011	22.0448	0.3034	127.2049
Frost filtered image	26.4070	20.7506	0.4214	135.5507
Enhanced Frost filtered image	27.0527	21.3963	0.4454	127.7399

TABLE 3: Comparison of speckle noise filtering techniques on a 512×512 Lena image corrupted by a Uniform speckle noise using an 11×11 window size.

	PSNR	S/MSE	CoC	ENL
Rayleigh noise				
Noisy image	19.4281	13.7718	0.1760	13.7621
Lee multiplicative filtered image	27.1461	21.4898	0.3158	106.4877
Kuan filtered image(NLOOK=ENL)	23.1365	17.4802	0.1256	34.0457
K.filtered image (Log. approximation)	27.3290	21.6726	0.3200	117.1893
K.filtered image (Poly. approximation)	27.3523	21.6960	0.3236	116.7191
Gamma filtered image	28.2304	22.5741	0.3979	230.0371
Frost filtered image	26.3868	20.7305	0.4231	240.8726
Enhanced Frost filtered image	27.0836	21.4272	0.4576	234.4497

TABLE 4: Comparison of speckle noise filtering techniques on a 512×512 Lena image corrupted by a Rayleigh speckle noise using an 11×11 window size.

	PSNR	S/MSE	CoC	ENL
Exponential noise				
Noisy image	20.0551	14.3987	0.1746	15.3187
Lee multiplicative filtered image	25.9639	20.3076	0.2597	67.2103
Kuan filtered image(NLOOK=ENL)	23.2500	17.5936	0.1368	34.4915
K.filtered image (Log. approximation)	27.2178	21.5614	0.3689	173.9484
K.filtered image (Poly. approximation)	27.1044	21.4480	0.3684	169.5444
Gamma filtered image	26.9633	21.2070	0.3179	101.6422
Frost filtered image	26.3943	20.7380	0.4299	238.9131
Enhanced Frost filtered image	27.0939	21.0376	0.4584	239.3688

TABLE 5: Comparison of speckle noise filtering techniques on a 512×512 Lena image corrupted by an Exponential speckle using an 11×11 window size.

Table 6 shows a comparison between the proposed adaptive Kuan filter and the basic and enhanced versions of Lee, Kuan, and Frost filters using five different images. It can be noticed that the optimal Kuan filter yields the highest PSNR, with the drawback of performing several filter runs in order to tune the filter to yield the best possible output quality. Furthermore, by setting the NLOOK parameter to ENL, Lee and Frost filters outperform the Kuan filter in their basic and enhanced versions. Moreover, our proposed solution approaches the performance of the optimal Kuan filter, with a negligible PSNR loss, and outperforms the basic and enhanced Lee and Frost filters, for all the speckled test images used in the filtering process.

PSNR	WomanD.H.	Pirate	Lena	CameraMan	LivingRoom
Noisy image	19.55	20.02	19.42	20.1	19.9
Lee	25.39	25.91	27.14	26.01	26.2
Frost	23.69	25.08	26.38	25.9	25.89
Enhanced Lee	25.61	26.01	27.30	26.78	26.88
Enhanced Frost	25.47	25.60	27.08	26.12	26.18
Kuan	23.34	24.21	24.02	24.92	25.1
Kuan (poly. approximation)	25.78	26.57	27.35	26.95	27.21
Kuan (log. approximation)	25.88	26.59	27.33	26.89	27.1
Kuan (optimal NLOOK)	25.92	26.70	27.44	27.11	27.35

TABLE 6: PSNR obtained with different despeckling filters using images of 512×512 size and an 11×11 filtering window.

It is important to note that in the literature [13, 14, 37], the Block Matching and 3D filtering (BM3D) algorithm is tested on images corrupted by additive noise. Moreover, the method's different parameters should be adequately chosen (depending on the noise strength, image size and percentage of edge pixels etc) in order to perform well dealing with speckle noise. Those parameters are the reference block size, the searching window size, the number of similar patches in the 3D block and the shrinking threshold. Therefore, finding the optimal set of parameters dealing with speckle noise is a very difficult task and choosing a non-optimal set of parameters usually fails to outperform traditional despeckling filters. On the contrary, the proposed adaptive filer can automatically estimate the suitable ENL parameter which will be used to spatially smooth the approximation image in the wavelet domain without need for many filter runs with different parameters.

Figure 9 shows a real spine lumbar MRI image obtained from [42], filtered with Enhanced Frost, Enhanced Lee, and the proposed adaptive Kuan filter using the polynomial approximation. A visual inspection of the results shows that all the filters succeed to reduce speckle noise and result in a pleasant visual appearance, preserving edges and contours. However, compared to our proposed solution, the enhanced Lee and Frost filters show over-blurred images.

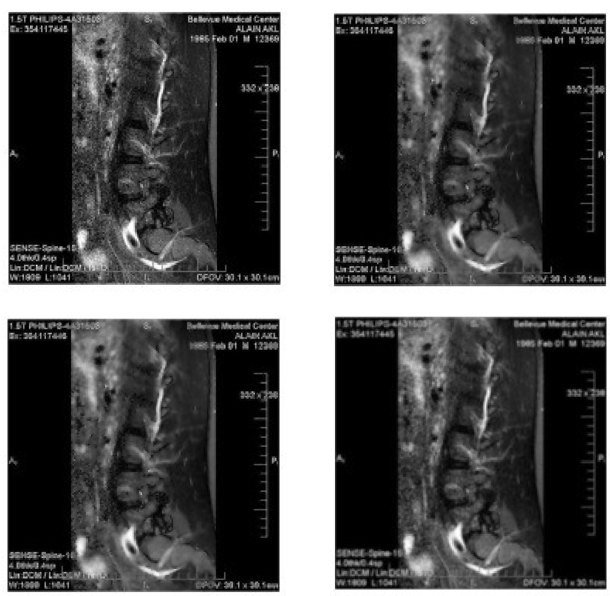

FIGURE 9: Spine lumbar MRI image [42]. Top left: original (noisy) image. Top right: Enhanced Frost filtered image. Bottom left: Enhanced Lee filtered image. Bottom right: result of filtering with our proposed solution using the polynomial approximation. A 13×13 window size is used for all the results.

Figure 10 shows a real cardiac catheterization speckled image obtained from [43], filtered with the enhanced versions of Frost and Lee and with the proposed Kuan filter (polynomial approximation). It can be observed that all the filters succeed to reduce speckle noise. However, the proposed adaptive Kuan filter outperforms the enhanced Frost and enhanced Lee filters in edge preservation. In other words, the Kuan filter with the proposed polynomial approximation yields visually better performance with the resulting image efficiently smoothed, while significantly preserving image details.

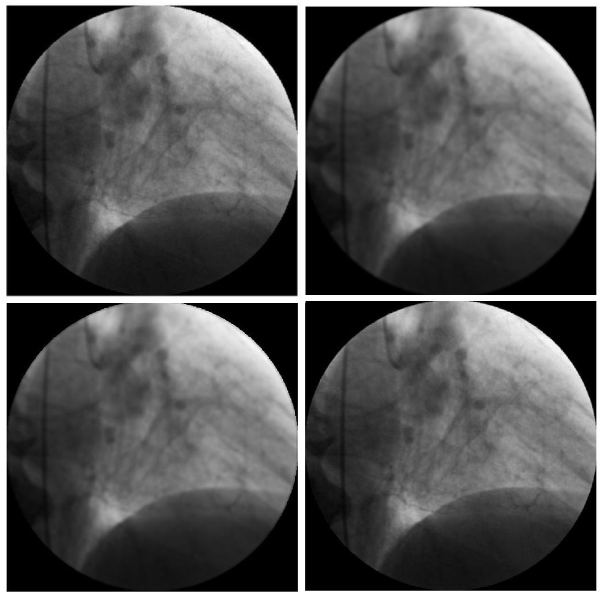

FIGURE 10: Cardiac catheterization image [43]. Top left: original (noisy) image. Top right: Enhanced Frost filtered image. Bottom left: Enhanced Lee filtered image. Bottom right: result of filtering with our proposed solution using the polynomial approximation. A 13×13 window size is used for all the results.

4.2 Performance of the Hybrid Wavelet-Spatial Despeckling Filter

This section deals with implementing the proposed hybrid wavelet-spatial domain filer. First, wavelet denoising with one decomposition level is applied on the 25 images of TID2013 database [39], each corrupted by 5 different levels of Gaussian speckle noise, then the results are compared to the same algorithm but using our enhanced Kuan filter to smooth the approximation image before wavelet reconstruction. We also apply wavelet denoising with the number of decomposition levels determined dynamically as proposed earlier, and compare the results to the same algorithm but using our enhanced Kuan filter to smooth the approximation image before wavelet reconstruction. Finally, the proposed enhanced Kuan filter is applied to the approximation image in each reconstruction level. Table 7 presents the gains (average, minimum, maximum, and standard deviation) with respect to the noisy image using different evaluation metrics (PSNR, CoC and ENL). It can be noticed that a Kuan smoothing on the approximation image with one decomposition level leads to an increase of 6.12 dB in average PSNR compared to 4.88 dB without the approximation image smoothing.

It is important to note that Kuan smoothing on the last decomposition level does not result in any significant enhancement. In fact, the smoothing strength of our adaptive Kuan filter depends on the NLK_AD parameter determined dynamically, which is very high in the approximation image of the last level, due to repetitive smoothing at every decomposition. Therefore, $W \approx 1$ (in (5)) and no filtering is performed in this case. Moreover, a Kuan smoothing filter on the approximation image of each level before reconstruction, leads to an increase of 0.2 dB in average PSNR compared to the case where approximation smoothing is performed only at the last decomposition level, without blurring the denoised image, which is obviously seen from the CoC metric.

Gaussian noise	Gains with respect to the noisy image											
	PSNR				CoC				ENL			
	AVG	MIN	MAX	STD	AVG	MIN	MAX	STD	AVG	MIN	MAX	STD
1L without Kuan smoothing	4.8808	3.0946	5.996	0.6681	0.0863	0.0143	0.0999	0.0121	21.2313	18.224	24.956	1.6711
1L with Kuan smoothing	6.1168	4.8226	6.9996	0.5514	0.0836	0.014	0.1089	0.013715	41.3668	29.2124	49.224	2.8868
Dynamic without Kuan smoothing	7.1225	5.826	7.9986	0.5538	0.1142	0.0543	0.971	0.079	60.0037	30.4054	65.2006	4.4478
Dynamic with Kuan smoothing on the last level	7.1228	5.8206	7.9991	0.5534	0.1153	0.0599	0.9174	0.0744	60.0042	30.4023	65.2505	4.4484
Dynamic with Kuan smoothing on all reconstructed levels	7.3229	5.9146	8.2906	0.556	0.1132	0.0443	0.9121	0.0742	64.7011	40.4054	72.3504	4.5485

TABLE 7: Evaluation metrics for wavelet-based denoising with and without Kuan smoothing. Sym1 wavelets and BayesShrink threshold selection technique are used.

4.3 Performance Evaluation for the Proposed Complexity Reduction Algorithm

In this section, the proposed accelerated algorithm is tested with different scenarios. *Figure 11* shows an example of the denoising results obtained using the Lena image corrupted by a Gaussian speckle of variance 3100, Haar, db4, sym4, and bior6.8 wavelets, Soft and Hard VisuShrink and BayesShrink.

The algorithm results in two wavelet decomposition levels. The first and second columns of *Figure 11* show the images obtained with one and two decomposition levels respectively. It can be seen that two decomposition levels give better performance than one decomposition level as expected. In addition, Universal Soft and Hard thresholding give more pleasant results than BayesShrink.

The same work is done with different standard test images, different noise variances and distributions, different thresholding methods, different wavelet types and families and using different decomposition levels, with images from [38, 39]. From our intensive test scenarios, we observed that a “best” denoising setup using wavelets cannot be generalized. In other words, there is no one optimal threshold selection technique and wavelet type that always give the best performance; performance depends on the wavelet thresholding algorithm, the wavelet family, the noise variance, the number of decomposition levels and the noisy image itself.

In the purpose of studying the complexity gain and PSNR loss when we stop at the estimated number of decomposition levels denoted *L_opt_algo*, we apply 10^4 times wavelet denoising on the images from TID2013 database [39] corrupted by five different levels of multiplicative Gaussian speckle noise, using BayesShrink threshold selection, ‘sym1’ wavelet type and different number of decomposition levels.

Figure 12 shows the histogram of the difference between the number of decomposition levels that yields the highest PSNR (i.e. to which we refer as “optimal”) and the number *L_opt_algo* obtained with our proposed method. It can be observed that 49% of the time, our algorithm successfully determines optimal number of levels whereas it performs 1 additional level for 11% of the time, and one and two levels less than the optimal number for 23% and 17% of the time, respectively. It is important to mention that these numbers could vary with a different dataset or simulation setup, but they give a general overview of the behavior of the proposed algorithm. As a result of erroneously estimating the optimal number of decomposition levels, some PSNR loss is incurred.

Figures 13 and *14* respectively show the histogram and the cumulative density function (CDF) of the PSNR loss due to the proposed algorithm. It can be observed that the loss does not exceed

0.04 dB and thus, can be considered as negligible. Therefore, the proposed acceleration algorithm has a good performance in terms of robustness against PSNR loss.

Figure 13 shows that there exists only 2% of no loss (loss of 0 dB), whereas *Figure 12* indicates that 49% of the images should have no loss, which could seem contradictory; in fact, referring to *Figure 14*, we notice that the PSNR loss is less than 0.01dB for 49% of the images, which can be explained to be due to numerical rounding errors in computer simulations and therefore the results in *Figures 13* and *14* are not contradictory but rather consistent with those in *Figure 12*.

FIGURE 11: Denoising using wavelets. 1st row: original image (left), speckled image (right). 2nd, 3rd and 4th row: db4 wavelet denoised images using the Universal Threshold with soft thresholding, the Universal Threshold with hard thresholding and with BayesShrink. Results obtained with one decomposition level are on the left and those obtained using two decomposition levels are on the right.

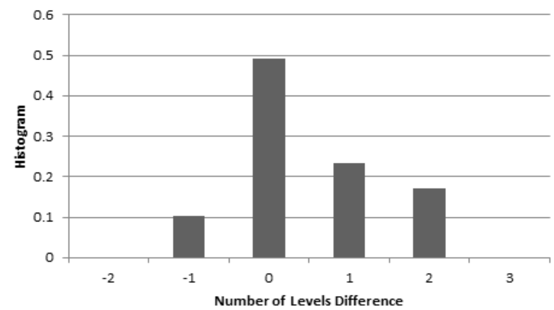

FIGURE 12: Histogram of the difference between *L_opt_algo* and the optimal number of decomposition levels.

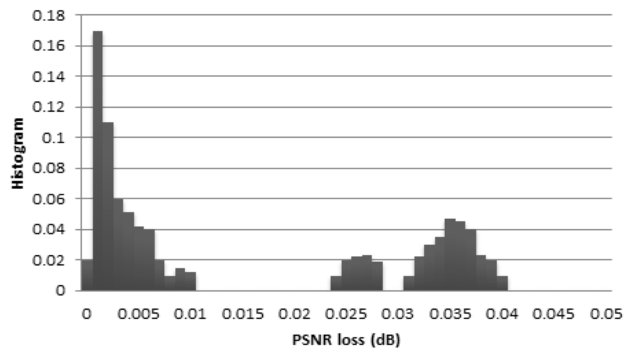

FIGURE 13: Histogram of the PSNR loss when using the acceleration algorithm.

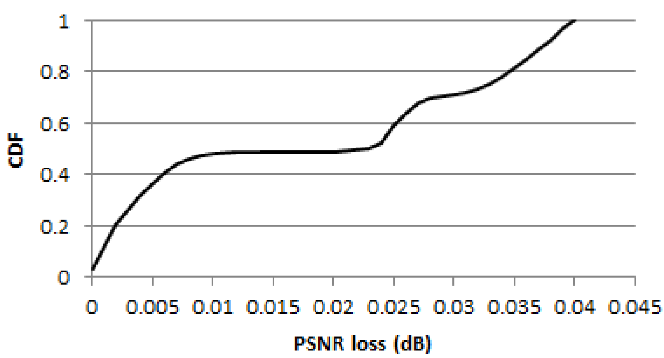

FIGURE 14: CDF of the PSNR loss when using the acceleration algorithm.

The advantage of the acceleration algorithm is the gain in complexity while keeping the PSNR loss negligible. In the purpose of analyzing this gain, the CPU time usage is computed for a number of ‘sym1’ wavelet decomposition levels followed by BayesShrink thresholding and the corresponding wavelet reconstruction. *Figure 15* shows the processor time usage (average of 100 runs) on a 2 GHz Intel Core 2 Duo CPU, for images from the TID2013 database [39], corrupted by 5 levels of multiplicative Gaussian speckle noise. The figure shows that one could save 0.12 microseconds per pixel by performing one decomposition level instead of two, and 0.10 microseconds per pixel for two levels instead of three. The incremental gain exponentially decreases as the number of decomposition levels increases, which is expected due to the size of the approximation image that is exponentially reduced (by a power of 2 in each dimension) for each additional level.

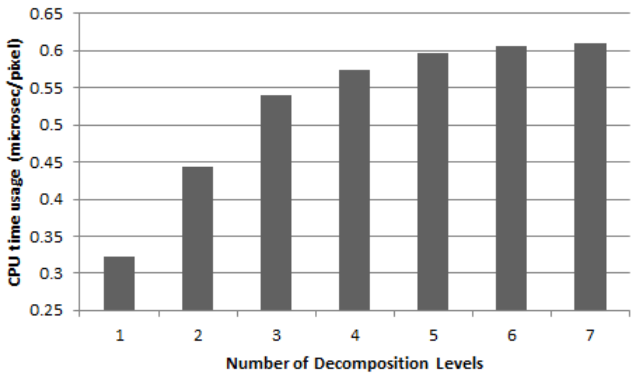

FIGURE 15: CPU time usage according to the number of decomposition levels.

5. CONCLUSION

We have proposed a hybrid wavelet-spatial denoising algorithm based on two-stage processing. An automatic parameter selection technique for the spatial Kuan filter is proposed in the first stage, which is later used to spatially smooth the approximation image of the wavelet coefficients in the second stage. An acceleration algorithm for wavelets computation is also proposed. It consists in selecting a suitable number of wavelet decomposition levels yielding near-optimal performance and eliminating the need for additional and unnecessary decomposition levels.

The procedures have been materialized on a set of different images under different conditions. In order to evaluate the quality of the results, objective metrics were used besides subjective ones identifying the method's capacity in reducing speckle noise. The obtained results quality was highly encouraging, in terms of speckle reduction and image characteristics preservation, and proved that the proposed acceleration algorithm is advantageous in complexity gain which suggests that further research in this direction could be promising, in particular in the optimal choice of the decomposition level where spatial smoothing can be performed on the approximation component.

The evaluation of repetitive runs of the spatial optimized filter is of our interest, to verify whether it allows for better noise suppression or reduction while critically preserving edges and texture. Moreover, it is known that smoothing is usually performed in a pre-processing phase before edge detection. In the proposed algorithm, edge detection was performed for the purpose of smoothing. Therefore, we propose the use of our enhanced Kuan filter recursively for the sake of edge detection. Finally, we aim at reinforcing the use of the proposed algorithm to enhance the performance of the BM3D denoising algorithm, leaving this perspective an open discussion for future considerations.

6. ACKNOWLEDGMENT

This work has been partly supported by a research grant from the Higher Center for Research at the Holy Spirit University of Kaslik (USEK), Lebanon.

7. REFERENCES

[1] A. Isar, S. Moga and D. Isar, "A new denoising system for SONAR images," *ACM Journal on Image and Video Processing*, January 2009.

[2] I. Shanthi and M.L. Valarmathi, "Speckle Noise Suppression of SAR Image using Hybrid Order Statistics Filters," *International Journal of Advanced Engineering Sciences and Technologies*, Vol. 5, No. 2, pp. 229-235, 2011.

[3] D. T. Kuan, "Adaptive Noise Smoothing Filter for Images with Signal Dependent Noise," *IEEE Trans. on Pattern Analysis and Machine Intelligence*, Vol. PAMI-7, No. 2, pp. 165-177, 1985

[4] D.H.H. Santosh, V.N.L. Kumar, D.R. Ramesh and P.S.Prasad, ‘’Efficient Techniques for Denoising of Speckle and Highly Corrupted Impulse Noise Images,’’ *IEEE Trans. Electronics Computer Technology (ICECT)*, Vol. 3, pp. 253-257, 2011.

[5] R. Ahirwar and A. Choubey, "A Novel Wavelet-based Denoising Method of SAR Image Using Interscale Dependency," *2011 International Conference on Computational Intelligence and Communication Systems*, Gwalior, India, October 2011.

[6] J. S. Lee, "Digital image enhancement and noise filtering by using local statistics," *IEEE Trans. on Pattern Analysis and Machine Intelligence*, vol. PAM1-2, 1980.

[7] J.S. Lee and I. Jurkevich, “Segmentation of SAR images,” *IEEE Trans. on Geoscience and Remote Sensing*, Vol. 27, No. 6, pp. 674-680, November 1989.

[8] J.S. Lee, “Speckle analysis and smoothing of synthetic aperture radar images,” *Computer Graphics and Image Processing*, Vol. 17, pp. 24-32, 1981.

[9] D. Kuan, A. Sawchuk, T. Strand and P. Chavel, “Adaptive restoration of images with speckle,” *IEEE Trans., Acoustic Speech, Signal Processing*, Vol. ASSP-35, No. 3, pp. 373-383, March 1987.

[10] A. Isar, S. Moga and D. Isar, "A new denoising system for SONAR images," *ACM Journal on Image and Video Processing*, January 2009.

[11] O.V. Michailovich and A. Tannenbaum, "Despeckling of medical ultrasound images," *IEEE Trans. on Ultrasonics, Ferroelectrics and Frequency Control*, pp. 64-78, January 2006.

[12] R. Ahirwar and A. Choubey, "A Novel Wavelet-based Denoising Method of SAR Image Using Interscale Dependency," *2011 International Conference on Computational Intelligence and Communication Systems*, Gwalior, India, October 2011.

[13] DabovKostadin, “Image and video Restoration with nonlocal transform-domain filtering,” *Ph.D. dissertation, Image/video restoration and enhancement*. Finland: Tampere University of technology, 2010.

[14] A. Buades, B. Coll, and J. M. Morel, “A non-local algorithm for image denoising,” *IEEE Trans. Comp. Vision. Pattern Reco.,* Vol.2, pp. 60-65, June 2005.

[15] Gonzales. Rafael C. and Woods. Richard E., “Digital Image Processing,” *Third Edition, Pearson Prentice Hall*, pp. 311-334, 346-356, 463-476, 488-509, 2008.

[16] C. Ju and C. Moloney, “An Edge-Enhanced Modified Lee filter for the Smoothing of SAR Image Speckle Noise,” *IEEE Workshop on Nonlinear Signal Image Processing*, Mackinac Island, MI, 1997.

[17] Himani Goyal, “Qualitative and Quantitative Evaluation of Image Denoising Techniques,” *International Journal of Computer Applications*, Vol. 8, No. 14, pp. 31-34, October 2010.

[18] D.M. Smith, “Speckle reduction and segmentation of Synthetic Aperture Radar images,” *International Journal of Remote Sensing*, Vol. 17, No. 11, pp. 2043-2057, 1996.

[19] L. V. Patil, K. K. Rane, A. P. Salvi, and S. S. Shitole, “Evaluation of Statistical Digital Image Filters,” *European Journal of Scientific Research*, June 2011.

[20] S.S. Ganugapati and C.R. Moloney, “A ratio based edge detector for speckled images based on maximum strength edge pruning,” *Proceedings of ICIP- 95, Washington, D.C.*, Vol. 2, pp. 165-168, October 1995.

[21] A. Lopes, E. Nezry, R. Touzi and H. Laur., “Maximum a posteriori speckle filtering and first order texture models in SAR images,” *Proceeding of Geoscience and Remote Sensing Symposium ‘90*, College Park, MD, Vol. 3, pp. 2409-2412, May 1990.

[22] Hong Sern Tan, “Denoising of Noise Speckle in Radar Image,” *B.E. Thesis*, School of Information Technology and Electrical Engineering, The University of Queensland, October 2001.

[23] L. Klaine, B. Vozel, and K. Chehdi. “Adaptive filtering of multiplicative noise by a new differential method*,” Proceeding of the Sixth International Symposium on Signal Processing and Its Applications’* 2003, July 2003.

[24] S. Aybike and S. B. Hasan, “Techniques of speckle noise reduction in ultrasound images,” *Proceeding of the 19th Signal Processing and Communications Applications Conference*, pp. 375-378, 2011.

[25] R. Rangarajan, R. Venkataramanan and S. Shah, “Image Denoising Using Wavelets: Wavelets & time frequency,” *Report*, December 16, 2002.
Available at: http://www-personal.engin.umich.edu/~rvenkata/551_code/Report.pdf

[26] Sani M. Isa, Ary Noviyanto and Aniati Murni Arymurthy, “Optimal Selection of Wavelet Thresholding Algorithm for ECG Signal Denoising,” *IEEE Trans. on Advanced Computer Science and Information System*, pp. 365-370, December 2011.

[27] I. Daubechies, “Ten lectures on wavelets,” *The Conference Board of the Mathematical Sciences*, *Series in Applied Mathematics*, Vol. 61, pp. 194-202, 1994.

[28] I. Daubechies, “Ten lectures on wavelets,” *The Conference Board of the Mathematical Sciences, Series in Applied Mathematics*, Vol. 61, pp. 198-202 and 254-256, 1994.

[29] I. Daubechies, “Ten lectures on wavelets,” *The Conference Board of the Mathematical Sciences, Series in Applied Mathematics*, Vol. 61, pp. 271-280.

[30] S. Mallat, “A theory for multiresolution signal decomposition: The wavelet representation,” *IEEE Trans., Pattern Anal. Machine Intell.,* Vol. 11, pp. 674–693, July 1989.

[31] S. Grace Chang, Bin Yu and Martin Vetterli, “Adaptive Wavelet Thresholding for Image Denoising and Compression,” *IEEE Trans on image processing*, Vol. 9, pp. 1532-1546, September 2000.

[32] David L. Donoho, “De-Noising by Soft-Thresholding,” *IEEE Trans. on information theory*, Vol. 41, No. 3, pp. 613-627, May 1995.

[33] Donoho, D.L., Johnstone, “Spatial adaptation by wavelet shrinkage,” *Biometrika, 81*, pp. 425-455, 1994.

[34] Shi Guangmin and Li Fudong, “Image Denoising with Optimized Subband Threshold,” *Proceeding of the Fifth International Conference on Computational Intelligence and Multimedia Applications*, 2003.

[35] Yunyi Yan, Baolong Guo, Zhanlong Yang and Xiang Fu, “Image Noise Removal via Wavelet Transform and r/K-PSO,” *Fourth International Conference on Natural Computation*, pp. 544-547, 2008.

[36] Aleksandra Pizurica and Wilfried Philips, “Estimating the Probability of the Presence of a Signal of Interest in Multiresolution Single- and Multiband Image Denoising,” *IEEE Trans. on image processing*, Vol. 15, No. 3, March 2006.

[37] K. Dabov, A. Foi, V. Katkovnik, and K. Egiazarian, “Image denoising by sparse 3D transform-domain collaborative filtering,” *IEEE Trans. Image Process.*, Vol. 16(8), pp. 2080-2095, August 2007.

[38] ImageProcessingPlace.com, Image Databases.

[39] TAMPERE IMAGE DATABASE 2013 TID2013, version 1.0.

[40] M. Misiti, Y. Misiti, G. Oppenheim, and J.M. Poggi, Matlab Wavelet Toolbox User’s guide version 3, 2005.

[41] A. Achim, A. Bezerianos and P. Tsakalides, “Ultrasound Image Denoising ViaMaximum A Posteriori Estimation Of Wavelet Coefficients,” *Proceedings of the 23rd annual international conference of the IEEE*, Vol. 3, pp. 2553-2556, 2001.

[42] M.R 12369 R_11_1200, Bellevue Medical Center, Mansourieh, El Metn, Lebanon.

[43] Interventional Cardiology Service, C07-372, N.D. Maritime hospital, Byblos, Lebanon.